Traveling wave solutions of lattice differential equations through an embedding approach

A.R. Humphries [1]

Department of Mathematics and Statistics, McGill University, Montreal, Quebec

R.P. Wilds [2]

Centre for Nonlinear Dynamics, McGill University, Montreal, Quebec

Abstract

A new method for obtaining planar Traveling Wave solutions to Lattice Differential Equations (LDEs) is presented. Traveling waves in LDEs are defined by mixed-type functional differential equations (FDEs) which are difficult to solve analytically or numerically. The FDE is transformed into the simpler problem of finding the fixed point of a system of ordinary differential equations, by a coordinate change and embedding in a larger problem. The approach is presented in a general form and then, to verify the method, is applied to a model problem for which an exact analytical solution is constructed. The solution structure of two new problems is then studied: a discrete reaction-diffusion equation with a tristable potential and the two-dimensional discrete Nagumo equation on a triangular lattice.

1 Introduction

Lattice Differential Equations (LDEs) are systems of coupled ODEs. They arise naturally in diverse fields including: biology [17,29,37], materials science [8,9], image processing [4,14], pattern recognition [15,16], and modeling of chemical reactions [6,20,24]. The survey papers [11,13,25], contain extensive references and lists of fields where LDEs occur.

Consider a general autonomous translationally invariant LDE

$$\dot{v_\eta}(t) = \mathcal{G}(\{v_{\eta+\zeta}(t)\}_{\zeta\in\Omega}) \qquad \eta, \eta+\zeta \subseteq \Gamma, v_\eta(t) \in \mathcal{E} \tag{1}$$

[1] Supported by a Canadian NSERC Discovery Grant
[2] Supported by a Canadian NSERC Postgraduate Scholarship

where $\Gamma \subseteq \mathbb{R}^p$ is a lattice consisting of a structured subset of $\mathbb{R}^p$, Ω is a set of shifts on the lattice, $\dot{}$ denotes component-wise differentiation with respect to t, and $\mathcal{E}$ is a normed vector space, which will usually be $\mathbb{R}^m$. Letting $v(t) = \{v_\eta(t)\}_{\eta\in\Gamma} \in X$ be the vector of states at time t and $v(t=0) = v^0$ the initial condition, and defining $\mathcal{G}_X = \{\mathcal{G}\}_{\eta\in\Gamma} : X \to X$ where X is a suitable Banach space, the initial value problem for (1) is well-posed (see [2,35]).

For notational simplicity we assume there are no nonlinear interactions between lattice sites. Our approach also applies to models with nonlinear inter-site interactions, and in [36] is successfully applied to an Ising model with such interactions. Assuming $\Gamma = \mathbb{Z}^p$ equation (1) can then be expressed as

$$\dot{v}_i(t) = \sum_{j\in\Omega} H_j(v_{i+j}(t)), \quad i, j \in \mathbb{Z}^p \tag{2}$$

where $H_j : \mathcal{E} \to \mathcal{E}$ and for $p > 1$, $i \in \mathbb{Z}^p$ is a p-tuple of coordinates. The use of $\Gamma = \mathbb{Z}^p$ does not restrict attention to the lattice $\mathbb{Z}^p$. Any lattice in $\mathbb{R}^p$ spanned by p linearly independent (primitive) vectors is represented by interpreting $i \in \mathbb{Z}^p$ as a set of coordinates along the primitive vectors. Let $\underline{i} \in \mathbb{R}^p$ denote the vector corresponding to the tuple i.

We consider planar traveling wave (TW) solutions to (2), which consist of a wave form $\varphi(\zeta) : \mathbb{R} \to \mathbb{R}$ that propagates across the lattice with constant velocity. Introducing a TW ansatz, $v_i(t) = \varphi(\zeta)$, where $\zeta = \underline{i} \cdot \underline{\sigma} - ct$, $c \in \mathbb{R}$ is the unknown wavespeed, and $\underline{\sigma} \in \mathbb{R}^p$ is a unit vector defining the propagation direction, and substituting into (2) yields the defining equations for such TWs;

$$-c\varphi'(\zeta) = \sum_{j\in\Omega} H_j(\varphi(\zeta + \tau_j)), \qquad \zeta \in \mathbb{R} \tag{3}$$

where $'$ denotes component-wise differentiation and $\tau_j = \underline{j} \cdot \underline{\sigma}$. Let φ^-, φ^+ denote homogeneous steady-state solutions of (2) and impose the boundary conditions $\varphi(\zeta \to \pm\infty) = \varphi^\pm$. Since (3) is translationally invariant a phase condition is required to specify a unique solution. Our numerical approach does not depend on the choice of phase condition, and so for simplicity of exposition we adopt the simple phase condition $\varphi(0) = \varphi^0$. Equation (3) may contain positive and negative shifts τ_j, (also referred to as advances/delays) which makes it a mixed-type Functional Differential Equation (FDE).

Although the above approach is analogous to finding TWs in a PDE via a TW ansatz, the propagation direction relative to the lattice results in a rich variety of direction-dependent phenomena, in contrast to PDEs where the propagation direction of a TW is generally irrelevant in a homogeneous medium. Also the presence of advances and delays in the FDE defining equation (3) makes analysis and computation of solutions much more difficult than the PDE case (where the TW defining equations are ODEs).

Traveling waves (TWs) are ubiquitous in the study of translationally invariant LDEs. For example, traveling wave solutions exist for the discrete Nagumo equation [38,39], discrete Fitzhugh-Nagumo equation [3,19], the nonlinear discrete Schrödinger equation [23], and coupled arrays of bistable oscillators [6,22,24]. Early work on mixed-type FDEs arising from traveling waves in LDEs can be found in [10,22,32,33]. More recently, Mallet-Paret [26,27] presented existence and uniqueness results for solutions in the scalar case $\mathcal{E} = \mathbb{R}$. In [12] asymptotic stability criteria were established for TW solutions to a large class of problems of the form (3).

There are few direct methods available for obtaining numerical solutions to (3). A sophisticated collocation boundary problem method is described in [1], which solves problems of the form (3) and generalisations, but it can be difficult to apply, as very accurate initial approximations to the solution $\varphi(\zeta)$ are often required for the algorithm to converge, and these are often not available for problems of interest. Less sophisticated methods for finding TWs, often used in applied sciences, largely rely on (2) possessing a stable TW which can in principle be found by numerically evolving (2) in time. In practice this poses new problems, since the computation must be performed on a finite domain and as the solution converges towards the TW it will propagate off the side of the computational domain. The traditional fix for this problem is to impose periodic-like boundary conditions, but this results in the computation of large period periodic solutions rather than TW solutions. These problems are all compounded in $\mathbb{R}^p$ for $p > 1$, where the direction of propagation is important.

We introduce a new approach based on a traveling coordinate change and embedding, rather than a traveling wave ansatz. Letting $x = \underline{i}\cdot\underline{\sigma} - \hat{c}t$ denote the traveling coordinate, with speed $\hat{c}$, and defining the waveform $u(x,t) = v_i(t)$, substitution into (2) yields

$$\frac{\partial u(x,t)}{\partial t} - \hat{c}\frac{\partial u(x,t)}{\partial x} = \sum_{j\in\Omega} H_j(u(x+\tau_j,t)), \qquad x \in \mathbb{R},\ t \in \mathbb{R}. \tag{4}$$

Note that (2) and (4) are not equivalent. For any $t > 0$, a solution $v_i(t)$ for $i \in \mathbb{Z}^p$ of (2) only defines $u(x,t)$ for discrete values of x, whereas in (4) the function $u(x,t)$ is defined for all $x \in \mathbb{R}$. Thus, in addition to the coordinate change we have effectively embedded the spatially discrete problem (2) in a spatially continuous problem (4). Nevertheless, in Section 2 we show that TW solutions of (2) are fixed points of the partial differential-difference equation (4) for suitable choice of the parameter $\hat{c}$. Thus the problem of finding a TW solution of (2) is reduced from finding a solution of the FDE (3) to finding a fixed point of the differential equation (4), which we do using two approaches. Firstly, if the TW solution of (2) is asymptotically stable it can be found by evolving (4) in time. Alternatively, we can solve directly for the fixed point of the differential equation (4). Variations of the traveling coordinate approach

have been reported previously [12,13] in other contexts, but have not been applied to derive numerical methods for spatially discrete problems before.

In Section 2 we describe the method in more detail, paying particular attention to the truncation to a finite computational domain and associated boundary conditions and functions. Section 3 applies the method to a spatially discrete Nagumo problem. We then derive a problem with an analytical solution and use it to analyse performance and convergence. The last two sections contain investigations into two new problems. In Section 4 we consider a one-dimensional discrete reaction-diffusion equation with a tristable potential and investigate the characteristics of traveling waves connecting the three minima of the potential. In Section 5 we analyse the discrete Nagumo equation on a two-dimensional triangular lattice. A previous study ([7]) analysed a variant of this problem on a square lattice, and we contrast the differences that the lattice structure introduces in the dynamics of traveling wave fronts.

2 Traveling Coordinate Method

Boundary conditions for (4) are obtained by generalising those for (3), resulting in $\lim_{x\to\pm\infty} u(x,t) = \varphi^{\pm}$ for all t, and the phase condition: $u(0,t) = \varphi^0$ for all t. We now establish the equivalence between TW solutions of (2) and (4).

Theorem 1 (Correspondence of Solutions) *A fixed point solution $u(x)$ of (4) with $\lim_{x\to\pm\infty} u(x) = \varphi^{\pm}$ is also a solution of (3) with $c = \hat{c}$ and $\lim_{\zeta\to\pm\infty} \varphi(\zeta) = \varphi^{\pm}$, and hence a TW solution of (2). Moreover, a traveling wave solution of (4) with speed s and $\lim_{x\to\pm\infty} u(x,t) = \varphi^{\pm}$ in the (x,t) coordinate frame is also a solution of (3) with $\lim_{\zeta\to\pm\infty} \varphi(\zeta) = \varphi^{\pm}$ and speed $c = \hat{c} + s$, and hence a TW solution of (2). The converses also hold, so that a solution of (3) with wave speed c is a fixed point of (4) when $\hat{c} = c$, and a travelling wave of speed $s = c - \hat{c}$ otherwise.*

PROOF. Applying the TW ansatz $u(x,t) = \psi(\rho)$ where $\rho = x - st$ to (4), yields

$$-(s+\hat{c})\psi'(\rho) = \sum_{j\in\Omega} H_j(\psi(\rho+\tau_j)) \tag{5}$$

which is the defining equation for a TW solution to (4) which moves at speed s in the (x,t) coordinate frame. Comparing (5) with (3), observe that if $c = s + \hat{c}$ then the equations are the same, and a solution of one solves the other. Furthermore, the specific case of $s = 0$ implies that $\psi(\rho)$ is a standing wave, or equivalently, $u(x,t)$ is a fixed point solution of (4). Thus, a fixed point solution of (4) has $u(x,t) = u(x) = \varphi(\zeta)$ with $c = \hat{c}$.

Following the theorem, our method for obtaining solutions $\varphi(\zeta)$ (and the wave speed c) to (3) is to find fixed points of (4), which we do using two methods. Firstly, if the solution $\varphi(\zeta)$ (or equivalently $\psi(\rho)$) is asymptotically stable, one can view (4) as being an initial value problem which evolves onto the traveling wave $\psi(\rho)$ as $t \to +\infty$. By adjusting $\hat{c}$ in (4) so that $u(x,t)$ is a stationary solution, the traveling wave and wave speed are obtained. Since the evolution is to a fixed point, not a TW solution, problems associated with the waveform propagating off the end of the computational interval do not arise with (4), in contrast to (2).

To find solutions which need not be asymptotically stable, one may find fixed point solutions of (4) by setting $\frac{\partial u}{\partial t}(x,t) = 0$ explicitly in (4). Numerically this will involve a discretisation of the steady state version of (4) and application of Newton's method.

Note that the second method encompasses the solutions amenable to the first method. However, the evolution approach is preferred when the TW is stable, as the basin of attraction of the TW is typically much larger than the ball of convergence for Newton's method. However, Newton's method converges after a few iterations, whereas the first approach can require a large number of numerical integrations to converge. Provided the TW is stable, a hybrid method that evolves an initial condition for a short time and then applies Newton's method yields the best convergence rate as a function of computational time.

2.1 Asymptotic Boundary Conditions

To solve (4) numerically, we truncate to a finite computational domain $x \in [L_-, L_+]$. But the shifts in (4) require knowledge of the solution over a larger region $x \in [L_- + \tau^-, L_+ + \tau^+]$, where $\tau^- = \min\{\tau_j\} < 0 < \max\{\tau_j\} = \tau^+$. Regarding solutions $u(x,t)$ as connecting orbits between homogeneous equilibria $\varphi^\pm$ of an infinite dimensional dynamical system, for $|L_\pm|$ sufficiently large information about solutions near $\varphi^\pm$ may be used to close the problem. However the method of projected boundary conditions (see eg [18]) is not applicable because both the stable and unstable manifolds of $\varphi^\pm$ are infinite dimensional.

We close the truncated problem by deriving asymptotic boundary conditions similarly to [1], where linear approximations to solutions of (3) for $|\zeta| \gg 0$ were obtained. However (4) is a partial differential-difference equation which poses serious challenges for such an analysis. But, since we will seek solutions of (4) which are either also solutions or are converging to solutions of (5), it is simpler to analyse the traveling wave equation (5) for $\psi(\rho)$ near $\varphi^\pm$, to obtain asymptotic boundary conditions. Linearising (5) about $\psi(\rho) = \varphi^-$, that is in

the limit $\rho \to -\infty$, let $\psi(\rho) = \varphi^- + \Psi(\rho)$, yielding

$$-(s+\hat{c})\Psi'(\rho) = \sum_{j\in\Omega} A_j^- \Psi(\rho+\tau_j), \tag{6}$$

where $A_j^- = J_{H_j}(\varphi^-)$ is the Jacobian of H_j evaluated at φ^-. Introducing the characteristic solution $\Psi(\rho) = \kappa e^{\rho\lambda}$, where $\kappa \in \mathcal{E}$ and $\lambda \in \mathbb{C}$, the characteristic equation is $0 = \det(\Delta^-(\lambda))$ where

$$\Delta^-(\lambda) = (s+\hat{c})\lambda I_m + \sum_{j\in\Omega} e^{\lambda\tau_j} A_j^-, \tag{7}$$

and I_m is the $m \times m$ identity matrix over $\mathcal{E}$. Recalling that the solution $\kappa e^{\lambda\rho}$ is to be valid in the regime $\rho \to -\infty$, we define

$$\Lambda^- = \{\lambda \in \mathbb{C} | \det(\Delta^-(\lambda)) = 0 \text{ and } \Re(\lambda) \geqslant 0\} \tag{8}$$

which yields the set of roots leading to bounded solutions $\Psi(\rho) = \kappa e^{\lambda\rho}$. A similar analysis for the linearisation about $\psi(\rho) = \varphi^+$ yields

$$\Lambda^+ = \{\lambda \in \mathbb{C} | \det(\Delta^+(\lambda)) = 0 \text{ and } \Re(\lambda) \leqslant 0\} \tag{9}$$

with Δ^+ defined similarly to (7) with $A_j^+ = J_{H_j}(\varphi^+)$. Thus the superpositions

$$\Psi^-(\rho) = \sum_{n=0}^{M^-} a_n^- e^{\lambda_n^-\rho}, \quad \lambda_n^- \in \Lambda^-, \qquad \Psi^+(\rho) = \sum_{n=0}^{M^+} a_n^+ e^{\lambda_n^+\rho}, \quad \lambda_n^+ \in \Lambda^+ \tag{10}$$

are solutions of the linearisation of (5) about $\psi = \varphi^-$ and φ^+, respectively, for any integer $M^\pm \geqslant 0$, and $a_n^\pm \in \mathcal{E}$ are arbitrary constants. It would be natural to expect that by incorporating additional $\lambda \in \Lambda^\pm$, in order of increasing $|\Re(\lambda)|$, then the asymptotic expansion (10) becomes a better approximation for $|\rho|$ large. But, under certain assumptions, Theorem 2.2 of [27] yields that if $s+\hat{c} \neq 0$ then there exists a unique $\lambda^- > 0$ such that $\lambda^- = \inf\{\Re(\lambda) | \lambda \in \Lambda^-\}$, and a unique $\lambda^+ < 0$ with $\lambda^+ = \sup\{\Re(\lambda) | \lambda \in \Lambda^+\}$. These roots will dominate the other roots in the superposition (10) in the limit as $\rho \to \pm\infty$ and so we set $M^\pm = 0$ and use the single dominant roots in (10).

Thus the linear approximations (10) lead to boundary functions (BFs), $u^\pm(x,t)$,

$$u^-(x,t) = \varphi^- + a^-(t)e^{\lambda^- x}, \quad x \leqslant L_-, \qquad u^+(x,t) = \varphi^+ + a^+(t)e^{\lambda^+ x}, \quad x \geqslant L_+$$

where the unknown functions of time $a^-(t), a^+(t)$ are determined by requiring continuity between $u(x,t)$ in the non-asymptotic regime and $u^\pm(x,t)$ at the domain boundaries $L_\pm$, giving

$$\begin{aligned} u^-(x,t) &= \varphi^- + (u(L_-,t) - \varphi^-)e^{\lambda^-(x-L_-)}, \quad x \leqslant L_-, \\ u^+(x,t) &= \varphi^+ + (u(L_+,t) - \varphi^+)e^{\lambda^+(x-L_+)}, \quad x \geqslant L_+ \end{aligned} \tag{11}$$

These BFs are also used to define boundary conditions (BCs) at $L_\pm$. Differentiating u^- with respect to x yields $\frac{\partial u^-}{\partial x}(x,t) = \lambda^-(u^-(x,t) - \varphi^-)$ and similarly for u^+. Thus, requiring $u(x,t)$ to have a continuous derivative with respect to x at the boundaries of the computational domain results in

$$\frac{\partial u}{\partial x}(L_-,t) = \lambda^-(u(L_-,t) - \varphi^-), \qquad \frac{\partial u}{\partial x}(L_+,t) = \lambda^+(u(L_+,t) - \varphi^+) \tag{12}$$

Using these BFs and BCs we truncate (4) so that the dynamics are entirely determined by values of $u(x,t)$ within the computational domain, resulting in

$$\frac{\partial u}{\partial t}(x,t) - \hat{c}\frac{\partial u}{\partial x}(x,t) = \sum_{j\in\Omega} h_j(u(x+\tau_j,t)), \qquad x \in [L_-, L_+] \tag{13}$$

where

$$h_j(u(x+\tau_j,t)) = \begin{cases} H_j(u(x+\tau_j,t)), & \text{if } x+\tau_j \in [L_-,L_+] \\ H_j(u^-(x+\tau_j,t)), & \text{if } x+\tau_j < L_- \\ H_j(u^+(x+\tau_j,t)), & \text{if } x+\tau_j > L_+ \end{cases} \tag{14}$$

with evaluation of the derivative $\frac{\partial u}{\partial x}$ at the boundaries $L_\pm$ given by the BCs (12). Equation (13) may be solved using standard methods for computing solutions to PDEs. In the following sections we will use the method of lines.

3 One-dimensional spatially discrete Nagumo equation

To demonstrate our approach for finding traveling wave solutions, consider a generalisation of the one-dimensional discrete Nagumo equation

$$\dot{v}_i(t) = v_{i+1}(t) - 2v_i(t) + v_{i-1}(t) - f(v_i(t)), \quad i \in \mathbb{Z} \tag{15}$$

In the notation of (2), $\Lambda = \mathbb{Z}$, $\mathcal{E} = \mathbb{R}$, $\Omega = \{-1, 0, 1\}$, and $H_j(\cdot)$ is given by

$$H_j(v_{i+j}) = \begin{cases} v_{i-1} & \text{if } j = -1 \\ -2v_i - f(v_i) & \text{if } j = 0 \\ v_{i+1} & \text{if } j = 1 \end{cases}$$

The nonlinearity $f(\cdot)$ is taken to be the derivative of a bistable potential which satisfies $f(0) = f(a) = f(1) = 0$ with $f'(0), f'(1) > 0$ and $f'(a) < 0$ where $a \in (0,1)$. The discrete Nagumo equation (15) has been the subject of much study [5,22,39,38]. It is one of the simplest equations which combines continuous time dependence with discrete spatial structure. The TW equation for (15) is

$$-c\varphi'(\zeta) = \varphi(\zeta+1) - 2\varphi(\zeta) + \varphi(\zeta-1) - f(\varphi(\zeta)) \tag{16}$$

where c is the unknown wavespeed. The asymptotic boundary conditions are $\varphi^- = 0$, $\varphi^+ = 1$, and the phase condition is specified by $\varphi^0 = a$. The traveling coordinate approach with $x = i - \hat{c}t$ and $u(x,t) = v_i(t)$ yields

$$\frac{\partial u}{\partial t}(x,t) - \hat{c}\frac{\partial u}{\partial x}(x,t) = u(x+1,t) - 2u(x,t) + u(x-1,t) - f(u(x,t)) \quad (17)$$

Zinner [39,38,21] showed that if $c \neq 0$ there exists a unique, monotonic, asymptotically stable TW solution of (16) which satisfies the given phase condition. The truncation of (17) is accomplished via the BFs (11) which become

$$\begin{aligned} u^-(x,t) &= u(L_-,t)e^{\lambda^-(x-L_-)}, && \text{for } x < L_- \\ u^+(x,t) &= 1 + (u(L_+,t)-1)e^{\lambda^+(x-L_+)}, && \text{for } x > L_+ \end{aligned} \quad (18)$$

where $\lambda^\pm$ are the real roots of the characteristic equations

$$0 = c\lambda^\pm + 2(\cosh(\lambda^\pm) - 1) - f'(\varphi^\pm), \quad (19)$$

with appropriate signs. The BCs (12) yield

$$\frac{\partial u}{\partial x}(L_-,t) = \lambda^- u(L_-,t), \qquad \frac{\partial u}{\partial x}(L_+,t) = \lambda^+(u(L_+,t)-1) \quad (20)$$

The truncated Nagumo problem may now be expressed as

$$\frac{\partial u}{\partial t}(x,t) = \hat{c}\frac{\partial u}{\partial x}(x,t) + h_{-1}(u(x,t)) - 2u(x,t) + h_1(u(x,t)) - f(u(x,t)), \quad x \in [L_-, L_+] \quad (21)$$

where $h_{-1,0,1}$ are defined via (3), (14) and the BCs are given by (20).

To solve (21) we employ the method of lines. Assume $\hat{c} > 0$ and partition the computational domain into N equal intervals of size $\Delta x = \frac{L_+ - L_-}{N}$ and let $u_j(t) \approx u(x_j,t)$ denote an approximation to the solution of (21) at $x = x_j \equiv L_- + j\Delta x$. $\underline{u}(t) = (u_0(t), u_1(t), ..., u_N(t))$ is the vector of approximations at time t. Furthermore, the quantity $\bar{u}(x,t)$ is defined to be a continuous function of x over $[L_-, L_+]$ at time t obtained by interpolating $\underline{u}(t)$. Spatially discrete versions of the functions h_{-1}, h_1, denoted by η_{-1}, η_1 are defined by

$$\eta_{-1}(u_j(t)) = \begin{cases} \bar{u}(x_j - 1, t), & \text{if } x_j - 1 \in [L_-, L_+] \\ e^{\lambda^-(x_j - L_-)}u_0(t), & \text{otherwise} \end{cases} \quad (22)$$

$$\eta_1(u_j(t)) = \begin{cases} \bar{u}(x_j + 1, t), & \text{if } x_j + 1 \in [L_-, L_+] \\ 1 + e^{\lambda^+(x - L_+)}(u_N(t) - 1), & \text{otherwise} \end{cases} \quad (23)$$

With these definitions, discretising the x-derivative yields

$$\dot{u}_j(t) = \hat{c}\delta_x(\underline{u}(t), x_j) + \eta_1(u_j(t)) - 2u_j(t) + \eta_{-1}(u_j(t)) - f(u_j(t)), \quad j \in [0, N] \tag{24}$$

where, for example, a second order 3-point assymetric difference (which avoids numerical instabilities that a centered discretisation introduces [34]) yields

$$\delta_x(\underline{u}(t), x_j) = \begin{cases} \lambda^- u_0(t), & \text{if } j = 0 \\ \dfrac{3u_{j+2}(t) - 4u_{j+1}(t) + u_j(t)}{2\Delta x}, & \text{if } j \in [1, N-2] \\ \dfrac{u_{j+1}(t) - u_j(t)}{\Delta x}, & \text{if } j = N-1 \\ \lambda^+(u_N(t) - 1), & \text{if } j = N \end{cases} \tag{25}$$

where at the $j = N-1$ point a first order discretisation is used for the derivative, and for $j = 0, N$ the boundary conditions (20) are employed.

This spatial discretisation of (21) may be compactly written as

$$\dot{\underline{u}}(t) = \underline{G}(\underline{u}(t)) \tag{26}$$

Regarding $\underline{u}(t)$ as an approximation to the solution $u(x,t)$ of (21) over the domain $[L_-, L_+]$, we introduce a norm which is a discrete approximation to the usual L^2 norm for continuous functions.

$$\|\underline{u}\|^2 = \Delta x \left(\frac{u_0^2 + u_N^2}{2} + \sum_{j=1}^{N-1} u_j^2 \right) \tag{27}$$

3.1 Finding Fixed Points

By Theorem 1, fixed points of (26) will give approximations to traveling waves $\varphi(\zeta)$ of (16). Additionally, since TW solutions of (16) are asymptotically stable, evolving (26) and adjusting $\hat{c}$ until $\dot{\underline{u}}(t) = 0$, yields these fixed points. Alternatively, setting $\dot{\underline{u}}(t) = 0$ explicitly in (26) results in a nonlinear system of equations to solve for the fixed point. We consider both approaches.

In the first approach, we employ explicit Runge-Kutta (RK) methods to numerically evolve (26) in time, and let $\underline{u}^n$ be the approximation to $\underline{u}(t_n)$ at time $t_n = n\Delta t$. For the second order approximation to the x-derivative used in δ_x (25), Heun's method is employed for the time discretisation.

To determine $\hat{c}$ so that $\underline{u}^n$ converges to a fixed point of (26), recall that $u(x,t)$ converges to a TW $\psi(\rho)$ and if $\hat{c} = c$ this is in fact a standing wave. Our algorithm operates in two stages. In the initial transient phase, the solution is evolved with fixed $\hat{c}$, and quickly converges to a neighbourhood of a TW of (15). In the second stage, the wavespeed s is determined by measuring the

movement of the wave on the mesh, and $\hat{c}$ is adjusted accordingly. Numerical evolution continues until $\|\underline{G}(\underline{u}^n)\|$ is below a specified tolerance.

An alternative to time evolution is to set $\dot{\underline{u}}(t) = 0$, and solve the resulting system of algebraic equations. Then there are $N+2$ unknowns u_i for $i = 0, \ldots, N$ and the wavespeed $\hat{c}$, with $N+1$ nonlinear equations arising form $0 = \underline{G}(\underline{u})$, and the phase condition $u(0) = a$ providing an additional condition. The resulting system of equations is solved using Newton's method.

In practice, we employ a hybrid method. With an initial mesh and solution guess, the Runge-Kutta method is used to evolve the solution close to the TW. Several iterations of Newton's method are then used to find the TW. If desired cubic-Hermite interpolation can be employed to define an approximate solution on a finer mesh, after which evolution by the RK method smoothes out residuals introduced in the interpolation process which could otherwise perturb the solution out of the Newton convergence region. Newton's method is again applied. This process is repeated until $\|\underline{G}(\underline{u})\|$ is sufficiently small ($< 10^{-8}$ unless otherwise indicated) on the desired final mesh.

3.2 Exact Solution

We now derive a problem with an analytical solution, using an inverse method similar to that employed in [1,30], which assumes a solution and then derives the problem which it solves. Motivated by the discrete Nagumo equation (16) we choose a solution φ_e and seek a function $f_e(\cdot)$ such that φ_e solves

$$-c_e\varphi_e'(\zeta) = \varphi_e(\zeta+1) - 2\varphi_e(\zeta) + \varphi_e(\zeta-1) - f_e(\varphi_e(\zeta)) \tag{28}$$

The nonlinearity $f_e(\varphi_e)$ may be implicitly solved for in (28), yielding

$$f_e(\varphi_e(\zeta)) = \varphi_e(\zeta+1) - 2\varphi_e(\zeta) + \varphi_e(\zeta-1) + c_e\varphi_e'(\zeta) \tag{29}$$

Requiring that the solution $\varphi_e(\zeta)$ satisfies the conditions

$$\lim_{\zeta\to-\infty}\varphi_e(\zeta) = 0, \quad \lim_{\zeta\to+\infty}\varphi_e(\zeta) = 1, \quad \text{and} \quad \varphi_e'(\zeta) > 0, \quad \forall\zeta\in\mathbb{R}$$

which are also satisfied by the solution of (16), results in the nonlinearity $f_e(\cdot)$ in (29) being well defined and ensures $f_e(0) = f_e(1) = 0$. To uniquely determine the wave speed c_e we require $f_e(a) = 0$, which is motivated by the cubic function: $f(v) = v(v-a)(v-1)$, commonly used in the Nagumo equation.

We now choose a generic form for the exact solution. Since numerical solutions

of (16) indicate that solutions often have a tanh-like profile we let

$$\varphi_e(\zeta) = \frac{1}{2^r}\left(\tanh\left(\frac{b\zeta}{2}\right)+1\right)^r = \left(\frac{e^{b\zeta}}{1+e^{b\zeta}}\right)^r \tag{30}$$

where $b, r > 0$ are parameters to be determined below. Using the second form of φ_e in (30), the shifted terms may be expressed as

$$\varphi_e(\zeta \pm 1) = \frac{\varphi_e(\zeta)e^{\pm br}}{(1+(e^{\pm b}-1)\varphi_e(\zeta)^{1/r})^r}. \tag{31}$$

Following a similar process the derivative term is found to satisfy

$$\varphi_e'(\zeta) = rb(1-\varphi_e(\zeta)^{1/r})\varphi_e(\zeta) \tag{32}$$

To determine b, r we require $f_e(\cdot)$ to have derivatives at 0 and 1 matching the cubic nonlinearity: $f_e'(0) = a$, $f_e'(1) = 1-a$ and make use of the characteristic equations arising from (28) (recall (19)) about $\varphi_e = 0, 1$ given by

$$0 = c_e\lambda^- + 2\cosh\lambda^- - 2 - a, \qquad 0 = c_e\lambda^+ + 2\cosh\lambda^+ - 2 - (1-a). \tag{33}$$

The dominant decay modes $\lambda^-, \lambda^+ \in \mathbb{R}$ are obtained explicitly from (30) as

$$\begin{aligned} \varphi(\zeta \to -\infty) &= 0 + e^{br\zeta} + \mathcal{O}(e^{b(r+1)\zeta}) \\ \varphi(\zeta \to +\infty) &= 1 - re^{-b\zeta} + \mathcal{O}(e^{-2b\zeta}). \end{aligned} \tag{34}$$

From (34) we identify $\lambda^- = br$ and $\lambda^+ = -b$. Substituting into (33) yields

$$0 = c_e br + 2\cosh(br) - 2 - a, \qquad 0 = -c_e b + 2\cosh b - 2 - (1-a) \tag{35}$$

which yields two equations for b and r. The condition defining the wave speed c_e is $f_e(a) = 0$, which combined with (30), (31), and (32) yields

$$c_e = \frac{1}{rb(1-a^{1/r})}\left(\frac{e^{br}}{(1+(e^b-1)a^{1/r})^r} - 2 + \frac{e^{-br}}{(1+(e^{-b}-1)a^{1/r})^r}\right) \tag{36}$$

Equations (35), (36) may be solved to yield b, r, c_e which then defines $f_e(\cdot)$ completely. Re-arranging (29) by making use of (31) and (32) we obtain

$$f_e(\varphi_e) = c_e br\varphi_e(1-\varphi_e^{1/r}) - \varphi_e\left(\frac{e^{br}}{[1+(e^b-1)\varphi_e^{1/r}]^r} - 2 + \frac{e^{-br}}{[1+(e^{-b}-1)\varphi_e^{1/r}]^r}\right) \tag{37}$$

3.3 Analysis using the exact solution

Two analyses of the methods of Section 3.1 for solving (17) are performed using the exact solution (30) with $f = f_e$ from (37). First, the effect of truncating (17) to a finite domain (21) is determined. The second analysis verifies that solutions of the discretisation of (21) converge to φ_e as $\Delta x \to 0$. All computations are performed with second order discretisation and have $a = 0.6$, from which we use (35) and (36) to obtain $b \approx 0.7, r \approx 1.0, c_e \approx 0.13$. The initial condition is set to

$$u(x,0) = \begin{cases} 0, & \text{if } x < -a \\ x + a, & \text{if } x \in [-a, 1-a] \\ 1, & \text{if } x > 1 - a \end{cases}$$

and the numerically computed solution is denoted by $\underline{\varphi}^*$. The norm defined in (27) is used with φ_e sampled at the mesh points.

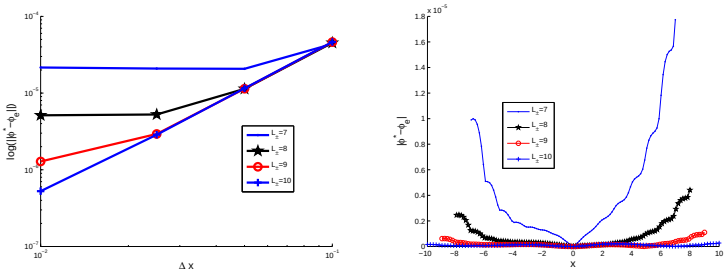

Fig. 1. (i) Loglog plot of error against mesh size Δx on various domains for the second order spatial discretisation. (ii) The difference $|\underline{\varphi}^* - \varphi_e|$ as a function of x over the computational domain for the various domain choices, with $\Delta x = 0.01$, showing the error distribution across the mesh.

Figure 1 shows the impact of the choice of the computational domain $[L_-, L_+]$ on the computational accuracy when solving (17) using the hybrid method of Section 3.1. For small $|L_\pm|$ the truncated problem (24) is a bad approximation to (17) with accuracy not increasing as the mesh size is decreased. However, for sufficiently large domains the solution converges with $\|\underline{\varphi}^* - \varphi_e\| \sim \Delta x^2$, consistent with the order of approximation. Figure 1(ii) shows that large errors at the boundaries are the main error source for small computational domains, but that the numerical approximation of the derivative in (25) quickly becomes the limiting factor, as the computational domain is enlarged. Figure 1(ii) also shows an asymmetry in the errors near $L_\pm$ which is likely due to the traveling wave nature of the problem.

Figure 2 shows the distribution of errors for the domain choices $[-15, 15]$ and $[-20, 20]$. The spatial distribution of errors is the same for corresponding mesh sizes Δx indicating that there is an optimal choice of $L_\pm$ beyond which further increases in domain size do not yield an increase in accuracy.

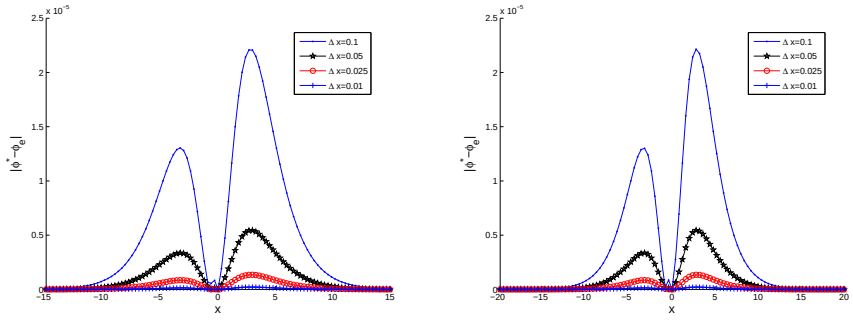

Fig. 2. $|\underline{\varphi}^* - \varphi_e|$ as a function of x for the domains (i) $[-15, 15]$ and (ii) $[-20, 20]$.

4 Tristable discrete reaction-diffusion equation

We now apply our approach to a one-dimensional discrete reaction-diffusion equation with a tristable potential. This may be viewed as a model of a lattice whose components can exist in one of three stable states. The continuous analog of this problem was studied in [31] where the co-existence of multiple states was analysed. We define

$$\dot{v}_i = v_{i+1} - 2v_i + v_{i-1} - \beta_q f(v_i) \tag{38}$$

where $f(v) = v(v-b)(v-1/2)(v-a)(v-1)$ with $0 < b < 1/2 < a < 1$ and $\beta_q \in \mathbb{R}^+$. Then f is the derivative of a tristable potential with $v = 0, 1/2, 1$ as the stable steady states. Traveling waves may be viewed as fronts propagating along the one-dimensional lattice in which the states at the lattice sites are transformed from one state to another as the wave travels. Applying the traveling wave ansatz: $\varphi(i - ct) = \varphi(\zeta) = v_i(t)$ yields

$$-c\varphi'(\zeta) = \varphi(\zeta + 1) - 2\varphi(\zeta) + \varphi(\zeta - 1) - \beta_q f(\varphi(\zeta)) \tag{39}$$

With the three steady-state solutions $\varphi = 0, 1/2, 1$, we choose to analyse traveling waves that connect: $\varphi^- = 0$ to $\varphi^+ = 1/2$ $(0 \to 1/2)$, $\varphi^- = 1/2$ to $\varphi^+ = 1$ $(1/2 \to 1)$, and $\varphi^- = 0$ to $\varphi^+ = 1$ $(0 \to 1)$ with the bracketed terms denoting the abbreviations that will be used. For the cases of $0 \to 1/2$ and $1/2 \to 1$ the solution behaviour will be analogous to that found for the Nagumo equation, since the solution only *sees* a restricted portion of the function f; however, the solution structure will depend on the two parameters a and b.

As in Section 3 we arrive at (21), but with quintic $f(\cdot)$. The method of lines is employed to reduce this to a system of ODEs: $\dot{\underline{u}}(t) = \underline{G}(\underline{u}(t))$. An initial solution is found using the hybrid method of Section 3.1. To study the solution structure as a, b, c are varied, we employ pseudo-arclength continuation to generate solution curves. All computations have $\beta_q = 10$ fixed and the second order discretisation with $\Delta x = 0.01$. The domain size $L_\pm$ is adaptively determined such that $|u_1 - \varphi^-| \sim 10^{-4}$ and $|u_N - \varphi^+| \sim 10^{-4}$. Convergence

criteria for the Newton iteration is set to be $\|\underline{G}(\underline{u})\| < 10^{-10}$.

We begin by studying the dependence of the solutions connecting $0 \to 1/2$ and $1/2 \to 1$ on the problem parameters. From these results we will be able to infer possible solutions connecting $0 \to 1$ to investigate. Figure 3 shows an

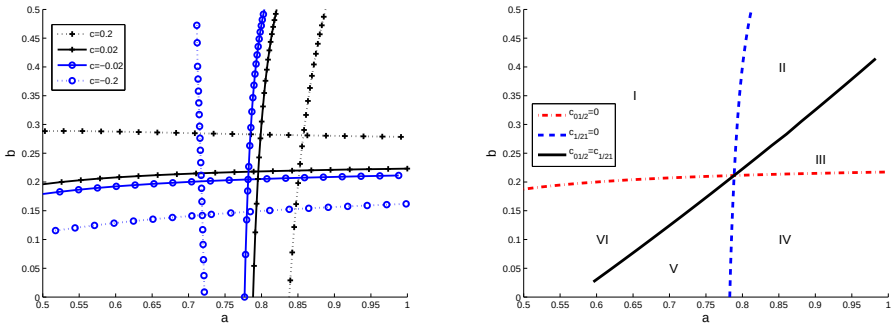

Fig. 3. Left: Contours of constant wave speed c (with $\beta_q = 10$) for TWs connecting $\varphi = 0$ to $\varphi = 1/2$ and $\varphi = 1/2$ to $\varphi = 1$. Right: A partition of the (a, b) plane. Above the $c_{0\frac{1}{2}} = 0$ curve the wavespeed for $0 \to 1/2$ waves is positive, and below it is negative. To the right of the $c_{\frac{1}{2}1} = 0$ curve $1/2 \to 1$ waves have positive wavespeed, and to the left negative. On the diagonal curve the wavespeeds of each wavetype are equal: $c_{0\frac{1}{2}} = c_{\frac{1}{2}1}$.

(a, b) phase portrait, with contours of constant wave speed for $0 \to 1/2$ and $1/2 \to 1$ solutions, and a partition of the (a, b) region which differentiates the relative values of the wave speeds for the two types of traveling waves. We observe a curve along which the $0 \to 1/2$ and $1/2 \to 1$ solutions have the same wave speed. Interestingly, calculations with other values of β_q indicate that the location of this curve appears to be independent of the value of β_q. Additionally, the location of the $c = 0$ contours for the two solutions $0 \to 1$, $1/2 \to 1$ may be approximated by finding the relationship between a and b that satisfies

$$\int_0^{\frac{1}{2}} f(x)dx = 0 \Rightarrow b = \frac{7a-2}{30a-7}, \qquad \int_{\frac{1}{2}}^1 f(x)dx = 0 \Rightarrow a = \frac{23b-18}{30b-23} \tag{40}$$

These conditions define curves in (a, b) along which $c = 0$ in the limit as β_q approaches 0 (the continuous case). For $\beta_q = 10$ there will be a strip about these curves that also have $c = 0$, however numerical calculations indicate that this region is very small ($< 10^{-2}$ in width). These conditions define six regions where the sign and magnitude of the two traveling wave speeds differ, as shown in Figure 3. From this we identify candidate regions for a connecting solution from $\varphi^- = 0$ to $\varphi^+ = 1$ to exist, based on whether the $0 \to 1/2$ and $1/2 \to 1$ waves have velocities which move away or towards each other. We first identify that in region IV no $0 \to 1$ connecting waves are possible since the $0 \to 1/2$ waves have negative speed (they move to the left in the ζ coordinate system) and the $1/2 \to 1$ wave have positive speed. Furthermore, the same argument

yields that regions III and V also have no $0 \to 1$ solutions, since although the $0 \to 1/2$ and $1/2 \to 1$ waves are moving in the same direction, the relative magnitudes result in these waves moving away from each other. In regions I, II and VI the wave speeds are such that the $0 \to 1/2$ and $1/2 \to 1$ solutions move towards each other. However, since $\varphi(\zeta) = 1/2$ is a stable steady-state solution then for all ζ such that $\varphi(\zeta) \approx 1/2$ the $0 \to 1$ solution tries to approach this constant value. These two opposing forces result in the component waves not passing through each other but instead forming a solution that connects $\varphi^- = 0$ to $\varphi^+ = 1$. The structure of $0 \to 1$ traveling waves is much richer than

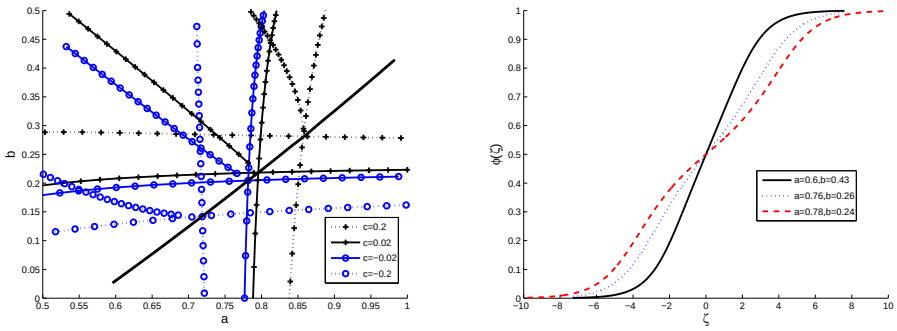

Fig. 4. Left: A reproduction of Figure 3 with curves of constant wavespeed for $0 \to 1$ added. The $0 \to 1$ curves terminate at the boundary curve along which $c_{0\frac{1}{2}} = c_{\frac{1}{2}1}$. Right: Waveforms from the $c = 0.02$ curve for $0 \to 1$ waves.

that observed for either of $0 \to 1/2$ and $1/2 \to 1$. The wavespeed of the $0 \to 1$ waves at a generic (a, b) coordinate is not simply related to the corresponding $0 \to 1/2$ and $1/2 \to 1$ waves. Also, $0 \to 1$ solutions are only seen above the $c_{0\frac{1}{2}} = c_{\frac{1}{2}1}$ boundary curve. Solutions connecting $0 \to 1$ near the boundary curve are difficult to obtain. Figure 4 augments the plot in Figure 3 to include the $0 \to 1$ results along with a selection of waveforms lying on the $c = 0.02$ curve. As the boundary curve is approached the waveform begins to separate into two waves. Numerical investigations indicate that the wave continues to separate as the curve is approached, with the $0 \to 1$ solutions never actually reaching the boundary curve.

5 Discrete Nagumo equation on a Triangular lattice

We now consider a discrete Nagumo equation on a two-dimensional lattice. The LDE may be viewed as a discretisation of the Nagumo equation,

$$\frac{\partial v}{\partial t}(x, y, t) = \Delta v(x, y, t) - f(v(x, y, t)) \tag{41}$$

where

$$\Delta v(x,y,t) = \frac{\partial^2 v}{\partial x^2}(x,y,t) + \frac{\partial^2 v}{\partial y^2}(x,y,t)$$

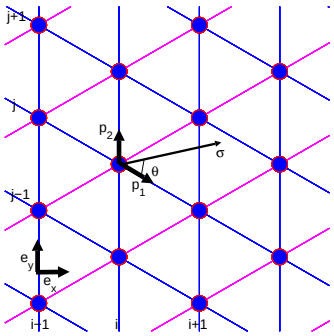

Fig. 5. Two-dimensional triangular lattice, with lattice sites indexed as shown, and the direction vector $\underline{\sigma}$ defined with the angle θ relative to $\underline{p}_1$. The primitive vectors $\underline{p}_1, \underline{p}_2$ of the lattice, and the rectangular Cartesian basis vectors $\underline{e}_x, \underline{e}_y$ are also shown.

In [7] a square lattice was investigated for the discrete Nagumo equation. Here we consider a triangular lattice as shown in Figure 5 with lattice spacing L. From the lattice structure we obtain an approximation $\tilde{\Delta}$ to the continuous Laplacian operator via a seven-point stencil approximation. With $\underline{e}_x, \underline{e}_y$ denoting the rectangular Cartesian basis vectors, the primitive vectors are defined as $(\underline{p}_1, \underline{p}_2) = (\frac{\sqrt{3}}{2}\underline{e}_x - \frac{1}{2}\underline{e}_y, \underline{e}_y)$. The lattice is indexed by the vector $\underline{i} = (i\underline{p}_1, j\underline{p}_2)$ where $(i,j) \in \mathbb{Z}^2$ as shown in Figure 5.

$$\tilde{\Delta} v_{i,j} = \frac{v_{i-1,j-1} + v_{i+1,j+1} + v_{i+1,j} + v_{i-1,j} + v_{i,j-1} + v_{i,j+1} - 6v_{i,j}}{\frac{3}{2}L^2} \tag{42}$$

Replacing the continuous Laplacian by the discrete one in (41) yields

$$\dot{v}_{i,j}(t) = \tilde{\Delta} v_{i,j}(t) - f(v_{i,j}(t)) \tag{43}$$

Multiplying through by $\beta_t \equiv \frac{3}{2}L^2$ and rescaling time results in

$$\dot{v}_{i,j} = v_{i-1,j-1} + v_{i+1,j+1} + v_{i+1,j} + v_{i-1,j} + v_{i,j-1} + v_{i,j+1} - 6v_{i,j} - \beta_t f(v_{i,j}) \tag{44}$$

Defining the direction vector $\underline{\sigma} = (\cos(\theta) + \frac{\sin(\theta)}{\sqrt{3}})\underline{p}_1 + \frac{2}{\sqrt{3}}\sin(\theta)\underline{p}_2$ as shown in Figure 5, where θ is measured counter-clockwise from the primitive vector $\underline{p}_1$, we introduce a traveling wave ansatz. Letting $\varphi(\underline{\sigma} \cdot \underline{i} - ct) = v_{i,j}(t)$, substitution into (44) yields

$$\begin{aligned} -c\varphi'(\zeta) = {} & \varphi(\zeta - \cos(\theta + \frac{\pi}{3})) + \varphi(\zeta + \cos(\theta + \frac{\pi}{3})) \\ & + \varphi(\zeta - \cos(\theta - \frac{\pi}{3})) + \varphi(\zeta + \cos(\theta - \frac{\pi}{3})) \\ & + \varphi(\zeta - \cos(\theta)) + \varphi(\zeta + \cos(\theta)) - 6\varphi(\zeta) - \beta_t f(\varphi(\zeta)) \end{aligned} \tag{45}$$

The homogeneous, stable states of (45) are the same as in Section 3, hence we seek traveling wave solutions that connect $\varphi^- = 0$ to $\varphi^+ = 1$ with the phase condition $\varphi^0 = a$. The same approach as used previously results in the set of ODEs $\dot{\underline{u}}(t) = \underline{G}(\underline{u}(t))$. The characteristic equation that arises in obtaining the boundary conditions/functions contains extra terms owing to the six shifts present in (45). The existence and uniqueness theory of [27] applies to (45), as well as the stability theory of [12], yielding that there exists a unique, asymptotically stable monotone traveling wave solution of (45). Solutions of (45) were obtained using the same approach as Section 4 with the second order discretisation. A mesh size of $\Delta x = 0.01$ is used for $c \geqslant 0.01$ computations and $\Delta x = 0.005$ when $c = 0.005$. $L_\pm$ are adaptively determined and the Newton iteration was considered to have converged once $\|\underline{G}(\underline{u})\| < 10^{-10}$.

We focus on the θ and β_t dependence of solutions to (45). Rather than reporting the value of a for given c, we work with the quantity $w(\theta, c) \equiv 2|a - \frac{1}{2}|$. Solutions of (45) are symmetric about $c = 0$ and $a = \frac{1}{2}$ and so the quantity w is the width of the interval centered on $a = \frac{1}{2}$ arising when solutions are obtained for c and $-c$. For example, fixing $\beta_t = 24$ and $\theta = 0$ one finds that with $c = 0.05$ then $a \approx 0.56$, and the solution with $c = -0.05$ has $a \approx 0.44$ and hence $w(0, 0.05) \approx 0.12$. The quantity w is especially useful when investigating the phenomena of propagation failure [28], [22] when $c = 0$ for $a \neq 1/2$, since $\lim_{c\to 0} w(\theta, c)$ defines the width of the interval of propagation failure.

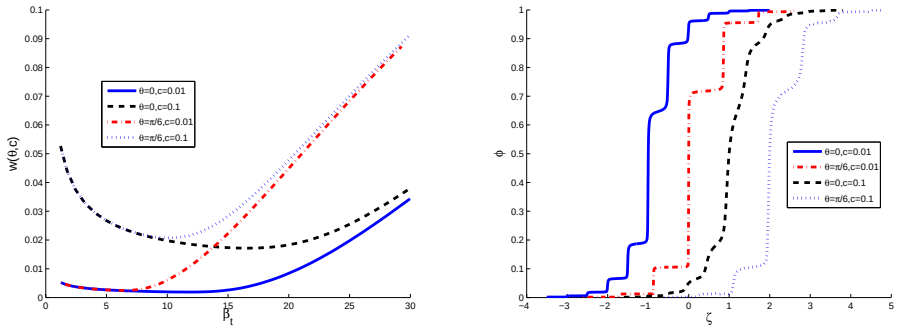

Fig. 6. Left: Dependence of $w(\theta, c)$ for $\theta = 0, \frac{\pi}{6}$ and $c = 0.01, 0.1$ as β_t is varied. Right: Computed wave forms (shifted for presentation) corresponding to the solutions at $\beta_t = 24$ in the left plot.

We begin by investigating dependence of the solution on β_t for the propagation directions $\theta = 0$ and $\theta = \frac{\pi}{6}$ with choices $c = 0.1$ and $c = 0.01$, as shown in Figure 6. From the left plot in Figure 6 we see that as β_t decreases the dependence of $w(\theta, c)$ on θ for the same c disappears. As β_t decreases it is equivalent to the lattice spacing L approaching 0, hence we obtain the continuous Nagumo equation, which does not have any directional dependence. For β_t increasing, numerical results for the one-dimensional discrete Nagumo equation (for instance [1], [36]) indicate that for large β_t, $\lim_{c\to 0} \frac{\partial a}{\partial c} \approx 0$, which implies that

w is approximately independent of c when c is near 0, consistent with Figure 6. The waveforms in the right plot of Figure 6 show the development of a step-like profile as c is decreased for the respective θ values. There are two significant differences between the $\theta = 0$ and $\theta = \pi/6$ solutions when $c = 0.01$. First, the width of the *steps* is larger for the $\theta = \pi/6$ solution than for the $\theta = 0$ solution. To understand this, set $c = 0$ in (45). The resulting difference equation will have monotonic solutions consisting of a series of horizontal step segments with discontinuous jumps. The step widths are determined by the shifts, which for $\theta = 0$ are $\{\pm 1/2, \pm 1\}$ leading to steps of width $1/2$, and for $\theta = \pi/6$ are $\pm\sqrt{3}/2$ giving steps of width $\sqrt{3}/2$. The second observation is that for $\theta = \pi/6$ the $c = 0.01$ solution is more step-like than the corresponding $\theta = 0$ one. To understand why the waveform features are different for the same c, we note that in propagation failure studies of the one-dimensional discrete Nagumo equation, the step-like shape of the solution depends both on how small c is, and on how large the interval of propagation failure is. Figure 7 shows that $\theta = \pi/6$ has a larger region of propagation failure than $\theta = 0$ and hence the solutions for $c = 0.01$ should be more step-like when $\theta = \pi/6$.

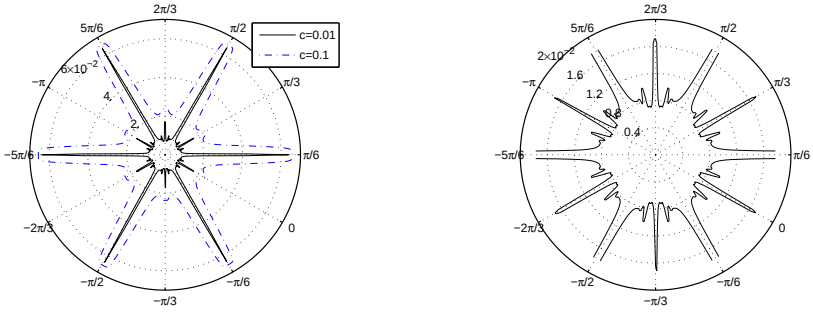

Fig. 7. Left: A polar plot of $w(\theta, c)$ for $c = 0.01$ and $c = 0.1$ with $\beta_t = 24$. Right: A magnified view near the origin with only the $c = 0.01$ curve shown.

To investigate the size of the interval of propagation failure, we consider the dependence of $w(\theta, c)$ on θ with $\beta_t = 24$ fixed and $c = 0.01$, as shown in Figure 7. The directional dependence of w and the $\frac{\pi}{6}$ symmetry of the lattice are clearly apparent. The following table shows numerical data for $w(\theta, c)$ as $c \to 0$ for $\beta_t = 24$ and $\theta = 0, \frac{\pi}{6}$.

	c=0.1	c=0.01	c=0.005	c=0
$\theta = 0$	0.0471	0.0343	0.0343	0.0343
$\theta = \frac{\pi}{6}$	0.1312	0.1275	0.1275	0.1275

Here, $w(\theta, 0)$ is approximated via extrapolation, under the assumption that

$\frac{\partial a}{\partial x} \to 0$ as $c \to 0$, and we see that $\theta = \frac{\pi}{6}$ does indeed have a larger region of propagation failure ($w(\theta, 0)$) than $\theta = 0$, as claimed above.

Mallet-Paret [28] showed that for a square two-dimensional lattice in the $c = 0$ limit the curve $w(\theta, c)$ is discontinuous at every θ for which $\tan(\theta)$ is rational, and continuous when $\tan(\theta)$ is irrational. The same result was also obtained in [7] with the nonlinearity $f(\cdot)$ given by the McKean caricature of the cubic. Figure 7 shows hints of this behaviour, based on the spiky shape of the curve at certain θ; however since the lattice is triangular, it is not clear if rational values of $\tan(\theta)$ are where to expect the curve to be discontinuous.

In [7] it is claimed that for a square lattice $w(\theta, 0)$ decreases with the interplanar spacing λ. Based on that result, we postulate that the curve $w(\theta, 0)$ is continuous at all values of θ such that $\lambda = 0$ and discontinuous at all non-zero λ. For our triangular lattice, the interplanar spacing is defined as follows. Let $(m, n) \in \mathbb{Z}^2$ be relatively prime, then the vector $m\underline{p}_1 + n\underline{p}_2$ defines the lattice plane direction, which is perpendicular to the propagation direction $\underline{\sigma}$, where the angle θ of $\underline{\sigma}$ measured relative to $\underline{p}_1$ is

$$\theta = \frac{\pi}{6} - \sin^{-1}\left(\frac{m}{2}\sqrt{\frac{3}{m^2+mn+n^2}}\right) = \frac{\pi}{6} - \cos^{-1}\left(\frac{m+2n}{2\sqrt{m^2+mn+n^2}}\right) \quad (46)$$

with corresponding interplanar spacing

$$\lambda = \frac{\sqrt{3}}{2\sqrt{m^2+mn+n^2}},$$

with $\lambda = 0$ for angles θ where (46) is not satisfied for any m, n. To test the postulated relationship for the triangular lattice, we investigate several λ. The largest possible λ are $\lambda = \sqrt{3}/2,\ 1/2,\ \sqrt{3}/2\sqrt{7},\ \sqrt{3}/2\sqrt{13}$ which correspond to $\theta = \pi/6,\ 0,\ \pi/6 - \sin^{-1}(\sqrt{3}/2\sqrt{7}),\ \pi/6 - \sin^{-1}(\sqrt{3}/2\sqrt{13})$. We see from Figure 7 that local maxima of $w(\theta, 0.005)$ clearly occur at the first few of these angles. To investigate whether the values of $w(\theta, 0.005)$ decrease in the order of decreasing λ consider the following table.

m, n	0,1	1,1	1,2	1,3	2,3	1,4
λ	0.8660	0.5	0.3273	0.2402	0. 1987	0.1890
θ	$\pi/6$	0	0.1901	0.2810	0.1150	0.3335
$w(\theta, 0.005)$	0.1178	0.0342	0.0198	0.0166	0.0138	0.0160

We see that $w(\theta, 0.005)$ does decrease in the order of decreasing λ, at least for the first four values. Thus we find evidence with a triangular lattice supporting the λ, θ relationship originally proposed in [7] for a square lattice. However we see that $\lambda(0.1150) > \lambda(0.3335)$, but that $w(0.1150, 0.005) < w(0.3335, 0.005)$,

which is not in the required order. It could be that the order changes in the limit as $c \to 0$, or that the numerically computed values are not sufficiently accurate, or the interplanar spacing argument might not be correct. We also have numerical evidence that the ordering may depend on β_t.

There is another explanation for the behaviour of (45) as θ is varied, which does not rely on θ being related to the direction of propagation across a lattice, but just considers the shifts in (45). There are no angles θ, for which all three shifts $\tau_1 = \pm\cos(\theta - \pi/3)$, $\tau_2 = \pm\cos(\theta)$ and $\tau_3 = \pm\cos(\theta + \pi/3)$ are rationally related. However, angles where two shifts are rationally related, occur precisely at the angles for which the interval of propagation failure is largest. The rational relationships are

$$n\tau_1 = m\tau_2 \quad \Longrightarrow \quad \theta = \tan^{-1}\left(\frac{2m-n}{\sqrt{3}n}\right),$$

$$n\tau_3 = m\tau_2 \quad \Longrightarrow \quad \theta = -\tan^{-1}\left(\frac{2m-n}{\sqrt{3}n}\right),$$

$$n\tau_1 = m\tau_3 \quad \Longrightarrow \quad \theta = -\frac{\pi}{6} + \tan^{-1}\left(\frac{\sqrt{3}n}{2m+n}\right).$$

Then taking $m = 1$, $n = 1$ the angles are: $\pm\pi/6$ and 0, and taking $m = 2$, $n = 1$ the angles are: 0 and $\sqrt{3}/2\sqrt{7}$, while for $m = 3$, $n = 1$ the angles are: $\pm\sqrt{3}/2\sqrt{7}$ and $\sqrt{3}/2\sqrt{13}$. So choosing angles such that $m + n$ is minimised results in the same ordering for the first few angles as before. However, it does not predict an ordering for the cases of $m = 4$, $n = 1$ and $m = 3$, $n = 2$ which caused difficulties before.

6 Conclusions

We have presented a new method for obtaining planar TW solutions to LDEs, based on a coordinate change and embedding in a larger problem. A finite difference approach is used to solve to solve the enlarged problem. The efficacy of the method is tested by applying it to a problem with a known exact solution, as well as to two new problems: a discrete reaction-diffusion equation with a tristable potential and the two-dimensional discrete Nagumo equation on a triangular lattice. For the tristable potential, the (parameter) region of existence of $0 \to 1$ waves was identified, and for the triangular lattice, we investigated the interplanar spacing spacing conjecture for the ordering of the directions with largest intervals of propagation failure and found evidence both for and against the conjecture. Note that although we solved (4) using finite differences, other techniques would be just as appropriate.

References

[1] K.A. Abell, C.E. Elmer, A.R. Humphries, and E.S. Van Vleck. Computation of mixed type functional differential boundary value problems. *SIAM J. Appl. Dyn. Sys.*, 4:755–781, 2005.

[2] V.S. Afraimovich and S.-N. Chow. Existence of evolution operators group for infinite lattice of coupled ordinary differential equation. *Dyn. Syst. Appl.*, 3:155–174, 1994.

[3] A.R.A. Anderson and B.D. Sleeman. Wave front propagation and its failure in coupled systems of discrete bistable cells modelled by FitzHugh-Nagumo dynamics. *Int. J. Bif. Chaos*, 5:63–74, 1994.

[4] D.G Aronson, M. Golubitsky, and J. Mallet-Paret. Ponies on a merry-go-round in a large array of josephson junctions. *Nonlinearity*, 4:903–910, 1991.

[5] J. Bell. Some threshold results for models of myelinated nerves. *Math. Biosci.*, 54:181–190, 1981.

[6] V. Booth, T. Erneux, and J.P. Laplante. Experimental and numerical study of weakly coupled bistable chemical reactors. *J. Phys. Chem.*, 98:6537–6540, 1994.

[7] J.W. Cahn, J. Mallet-Paret, and E.S. Van Vleck. Traveling wave solutions for systems of ODE's on a two-dimensional spatial lattice. *SIAM J. Appl. Math.*, 59:455–493, 1998.

[8] A. Carpio and L. L. Bonilla. Discrete models of dislocations and their motion in cubic crystals. *Phys. Rev. B*, 71(13):134105, 2005.

[9] A. Carpio, L.L. Bonilla, and G. Dell'Acqua. Motion of wave fronts in semiconductor superlattices. *Phys. Rev. E*, 64:036204, 2001.

[10] H. Chi, J. Bell, and B. Hassard. Numerical solution of a nonlinear advance-delay-differential equation from nerve conduction theory. *J. Math. Biol.*, 24:583–601, 1986.

[11] S.-N. Chow and J. Mallet-Paret. Pattern formation and spatial chaos in lattice dynamical systems: I. *IEEE Trans. Circuits Systems I Fund. Theory Appl.*, 42:746–751, 1995.

[12] S.-N. Chow, J. Mallet-Paret, and W. Shen. Traveling waves in lattice dynamical systems. *J. Diff. Eqn.*, 149:248–291, 1998.

[13] S.-N. Chow, J. Mallet-Paret, and E.S. Van Vleck. Dynamics of lattice differential equations. *International Journal of Bifurcation and Chaos*, 6:1605–1622, 1996.

[14] L.O. Chua and T. Roska. The CNN paradigm. *IEEE Trans. Circuits Syst.*, 40:147–156, 1993.

[15] L.O. Chua and L. Yang. Cellular neural networks: Applications. *IEEE Trans. Circuits Syst.*, 35:1273–1290, 1988.

[16] L.O. Chua and L. Yang. Cellular neural networks: Theory. *IEEE Trans. Circuits Syst.*, 35:1257–1272, 1988.

[17] G. Cocho and G. Martinez-Mekler. On a coupled map lattice formulation of the evolution of genetic sequences. *Phys. D*, 51:119–130, 1991.

[18] J.W. Demmel, L. Dieci, and M.J. Friedman. Computing connecting orbits via an improved algorithm for continuing invariant subspaces. *SIAM J. Sci. Comput.*, 22:81–94, 2000.

[19] C.E. Elmer and E.S. Van Vleck. Spatially discrete fitzhugh-nagumo equations. *SIAM J. Appl. Math.*, 65:1153–1174, 2005.

[20] T. Erneux and G. Nicolis. Propagating waves in discrete bistable reaction-diffusion systems. *Phys. D*, 67:237–244, 1993.

[21] D. Hankerson and B. Zinner. Wavefronts for a cooperative tridiagonal system of differential equations. *J. Dynam. Diff. Eqn.*, 5:359–373, 1993.

[22] J.P. Keener. Propagation and its failure in coupled systems of discrete excitable cells. *SIAM J. Appld. Math.*, 47:556–572, 1987.

[23] P. G. Kevrekidis, K. O. Rasmussen, and A. R. Bishop. The discrete nonlinear schrodinger equation: A survey of recent results. *Int. J. Mod. Phys. B*, 15(21):2833–2900, 2001.

[24] J.P. Laplante and T. Erneux. Propagation failure in arrays of coupled bistable chemical reactors. *J. Phys. Chem.*, 96:4931–4934, 1992.

[25] J. Mallet-Paret. Spatial patterns, spatial chaos, and traveling waves in lattice differential equation. In *Stochastic and spatial structures of dynamical systems*, pages 105–129. 1996.

[26] J. Mallet-Paret. The Fredholm alternative for functional differential equations of mixed type. *J. Dyn. Diff. Eqn.*, 11:1–48, 1999.

[27] J. Mallet-Paret. The global structure of traveling waves in spatially discrete dynamical systems. *J. Dyn. Diff. Eqn.*, 11:49–128, 1999.

[28] J. Mallet-Paret. Crystallographic pinning: Direction dependent pinning in lattice differential equations. *To appear in JDE*, 2006.

[29] R.E. Mirollo and S.H. Strogatz. Synchronization of pule-coupled biological oscillators. *SIAM J. Appl. Math.*, 50:1645–1662, 1990.

[30] M. Rodrigo, C. Elmer, and R.M. Miura. A construction technique for heteroclinic solutions to continuous and differential-difference damped wave equations. *CAMS Technical Report 0203-24, NJIT*, 2003.

[31] J. Rubinstein, P. Sternberg, and J. B. Keller. Front interaction and nonhomogeneous equilibria for tristable reaction-diffusion equations. *SIAM J. Appl. Math.*, 53(6):1669–1685, 1993.

[32] A. Rustichini. Functional differential equations of mixed type: the linear autonomous case. *J. Dyn. Diff. Eqn.*, 1:121–143, 1989.

[33] A. Rustichini. Hopf bifurcations for functional differential equations of mixed type. *J. Dyn. Diff. Eqn.*, 1:145–177, 1989.

[34] G.D. Smith. *Numerical Solution of Partial Differential Equations.* Clarendon Press, Oxford, 3rd edition, 1985.

[35] B. Wang and E.S. Vleck. Attractors for lattice Fitzhugh-Nagumo systems. *Physica D*, 212:317–336, 2005.

[36] R.P. Wilds. A new approach for obtaining traveling wave solutions to lattice differential equations. Master's thesis, McGill University, 2005.

[37] R.L. Winslow, A.L. Kimball, A. Varghese, and D. Noble. Simulating cardiac sinus and atrial network dynamics on the connection machine. *Phys. D*, 64:281–298, 1993.

[38] B. Zinner. Stability of traveling wavefronts for the discrete Nagumo equation. *SIAM J. Math. Anal.*, 22:1016–1020, 1991.

[39] B. Zinner. Existence of traveling wavefront solutions for the discrete Nagumo equation. *J. Diff. Eqn.*, 96:1–27, 1992.